Quantum Information Processing, Vol. 3, No. 6, December 2004 (© 2004)

Geometric Approach to Digital Quantum Information

Chad Rigetti[1,3], Rémy Mosseri[2] and Michel Devoret[1]

Received June 28, 2004; accepted September 21, 2004

We present geometric methods for uniformly discretizing the continuous N-qubit Hilbert space H_N. When considered as the vertices of a geometrical figure, the resulting states form the equivalent of a Platonic solid. The discretization technique inherently describes a class of $\pi/2$ rotations that connect neighboring states in the set, i.e., that leave the geometrical figures invariant. These rotations are shown to generate the Clifford group, a general group of discrete transformations on N qubits. Discretizing H_N allows us to define its digital quantum information content, and we show that this information content grows as N^2. While we believe the discrete sets are interesting because they allow extra-classical behavior—such as quantum entanglement and quantum parallelism—to be explored while circumventing the continuity of Hilbert space, we also show how they may be a useful tool for problems in traditional quantum computation. We describe in detail the discrete sets for one and two qubits.

KEY WORDS: Quantam computation; quantum gates; stabilizer codes; dense lattice.
PACS: 03.67.Lx; 03.67.pp; 03.67.-a; 03.67.Mn.

1. INTRODUCTION

The discrete nature of the configuration space for N classical bits is the key property allowing robustness of digital computation. The Hilbert space H_N for N qubits, on the other hand, is a *continuous* complex manifold. This continuity appears essential to the exponential speed-up of some quantum computing algorithms, such as Shor's factoring algorithm[(1)], over their classical counterparts[4]. But it also poses a challenging problem for the experimentalist: errors in quantum gates are themselves continuous, so

[1]Department of Applied Physics, Yale University, New Haven, Connecticut 06520-8284, USA
[2]Groupe de Physique des Solides, Université Paris VI, campus Boucicaut, 140 rue de Lourmel, 75015 Paris, France
[3]To whom correspondence should be addressed. E-mail: chad.rigetti@yale.edu
[4]As evinced by the Gottesman–Knill theorem, for example. See Ref. [(11)].

1570-0755/04/1200-0351/0

even minute errors can accumulate throughout the execution of an algorithm and lead to its failure.

Yet, quantum error correction and fault-tolerant computation schemes have been developed to meet this challenge[2–4]. That reliable quantum computation is possible using both a noisy quantum register and noisy gates is a result of surpassing importance. However, such schemes still place stringent fidelity requirements on the basic quantum gates and the quantum register: estimates for the threshold error probability above which they fail are typically 10^{-5}–10^{-6}[5].

Can universal control of a scalable quantum register with this level of fidelity be realized? If so, are there concepts we can borrow from digital computation that might facilitate the development of this technology? If not, are there "intermediate" computational paradigms that might relax these requirements, but still exploit "extra-classical" phenomena such as quantum parallelism and quantum entanglement? We note that these are still possible in a *discrete* Hilbert space.

Quantum gates are implemented by applying time-dependent fields to the qubits. They correspond to rotations of a unit vector in H_N, with the angle of rotation usually determined by the duration and amplitude of the pulse which generates the field. In principle, such rotations are simple to implement, given an appropriate time-dependent Hamiltonian. But in practice, noise in both the qubit system and applied fields inevitably leads to errors. Sophisticated techniques that build up a desired gate from a sequence of rotations about successively orthogonal axes have been developed to mitigate the effects of noise. In the field of NMR, especially, techniques for performing high-fidelity rotations are now very mature[6]. Yet such techniques for protecting against noise are not directly generalizable to arbitrary angles and axes of rotation. As a result, most experimental protocols for quantum manipulations rely as heavily as possible on a small set of rotations, usually by an angle of $\pi/2$ or π, specifically optimized for the given qubit system. In the landmark experiment by Vandersypen *et al.*, in which an NMR-based quantum processor was used to factor the number fifteen via Shor's algorithm, the protocol contained a single rotation by an angle less than $\pi/2$—a conditional $\pi/4$ rotation[7].

Nonetheless, universal control of a quantum register requires in theory only a finite number of discrete gates, provided the gates form a universal set. Then an arbitrary "software-level" quantum gate can be constructed to a precision ϵ by concatenating $\mathcal{O}(\log^c(1/\epsilon))$ discrete gates from the universal set ($c \approx 2$)[5]. However, given that each discrete gate itself would likely comprise a sophisticated series of rotations, the prospect of concatenating $\mathcal{O}(\log^c(1/\epsilon))$ such gates to create each software-level

operation—and doing so before the register decoheres—makes the fidelity requirements of fault-tolerant computing schemes all the more exacting.

Much of this difficulty in achieving high-fidelity control of a quantum register can be alleviated by limiting ourselves to *non-universal* sets of quantum gates which generate only *finite* transformation groups. A finite transformation group implies a finite number of possible states, so this is equivalent to imposing a discretization on the underlying Hilbert space: the quantum register becomes "digital". By suitably choosing the transformation group, the allowed states can be selected to have certain well-defined properties, such as known expectation values with respect to a set of measurement operators.

As an illustration of this idea, consider the task of testing the experimental protocol for generating one-qubit rotations, which can be represented on the Bloch sphere. Suppose we wish to optimize the fidelity of a $\pi/2$ rotation about the y-axis in a given qubit system. Starting from the state $|0\rangle$, we perform a counter-clockwise $\pi/2$ rotation about the y-axis, yielding the target state $|+x\rangle = (|0\rangle + |1\rangle)/\sqrt{2}$, then we perform a measurement in the $\{|0\rangle, |1\rangle\}$ basis. By repeating this many times, we obtain the expectation value $\langle\sigma_z\rangle$ of the target state $|+x\rangle$. Assuming imperfections in the state preparation and readout have been accounted for, this expectation value would approach zero if our $\pi/2$ gate were perfect, since $\langle +x|\sigma_z|+x\rangle = 0$, while deviations from zero would imply an imperfect $\pi/2$ gate. Specifically, $\langle\sigma_z\rangle = \delta$ would imply that, on average, the gate has performed a rotation by an angle of $2\arccos\sqrt{(\delta+1)/2}$. With knowledge of other one-qubit discrete states and their expectation values $\langle\sigma_i\rangle$, we could also test rotations about the x- and z-axes. By direct generalization, this simple protocol can be used to test rotations on any number of qubits, provided we have an appropriate discrete set of target states.

Also, in the nascent field of quantum feedback control, techniques have been developed to *dynamically* correct quantum processes. By performing continuous weak measurements on the quantum system, it is possible to control and correct quantum state evolution through feedback[8,9]. Incorporating these techniques into quantum computing experiments could also be facilitated if the number of processes involved were reduced to include only a small class of rotations connecting states with well-defined properties.

Having explained why we wish to consider a discrete subset of the full continuous Hilbert space, we would now like to draw a geometrical analogy. Since we do not want to privilege any region of Hilbert space over any other, the set must comprise a uniform sampling of H_N. The structure of the finite sets we have in mind is exemplified in real space

by the Platonic solids—geometrical figures such as the tetrahedron, cube and octahedron characterized by the geometric equivalence of their vertices—which represent discrete subsets uniformly spanning a sphere in $\mathbb{R}^3$. In short, we are seeking to generalize the Platonic solids to Hilbert space by selecting from H_N a finite set of states corresponding to the vertices of a 2^N-dimensional complex uniform polytope. We call such subsets *uniform Hilbertian polytopes,* and denote them by $\mathfrak{H}_N$.

In discretizing an N-qubit register, what extra-classical phenomena must be sacrificed? If we select the transformation group to include only π rotations—the quantum generalizations of the NOT gate—we generate only a discrete set of 2^N states, and fall back on a purely classical register, with no possibility for quantum entanglement. But, as we will show, the next level towards finer rotations, the transformation group based on $\pi/2$ rotations, is sufficient for rich extra-classical behavior: the number of discrete states in the set then grows as $2^{(N^2+3N)/2}$, the majority of which are entangled for $N > 2$. Also, the super-extensive growth of the discrete set relative to the classical number of states 2^N implies that a great deal of the quantum parallelism possible in the full Hilbert space remains possible in the discrete set. Though such a digital quantum register would not allow algorithms which are exponentially faster than their classical counterparts (Gottesman–Knill theorem), a possible reduction of an algorithmic scaling speed from $O(N^2)$ to $O(N)$ could still be useful.

At the same time, within the framework of traditional quantum computation, a discrete set and its associated transformation group can provide a useful "roadmap" for navigation in the entire Hilbert space.

The notion of discrete sets of N-qubit states is not novel. Indeed, discrete sets have already been considered in quantum error-correcting codes. There, a special set of 2^k orthogonal states, to be used as codewords for the basis states of k encoded qubits, are selected from a higher-dimensional continuous space H_N. Gottesman's stabilizer formalism provides a general framework for describing and producing quantum error-correcting codes, and allows an analysis of a broad class of quantum networks in the Heisenberg picture[11,12]. Powerful though it is, the stabilizer formalism approaches the problem of discretization algebraically; it does not address the geometric relationship between the discrete quantum states, nor the relationships among the various gates that connect these states.

The purpose of this paper is thus to provide such a geometric approach to the uniform discretization of H_N, and to suggest the use of such discrete sets, either as an arena for exploring extra-classical behavior, or as a heuristic tool for the analysis of certain quantum information

processing problems. We refer to these notions collectively as *digital quantum information*[5].

For simplicity, we focus here on the one- and two-qubit Hilbert spaces. However, most of our results are directly generalizable to higher-dimensional spaces. When possible, we use a language that makes this generalization straightforward, if tedious. In Section 2, we treat the discretization problem using stabilizer theory and derive a class of generalized $\pi/2$ rotations belonging to the Clifford group that connect states in the discrete set. Later in Section 3, we present an alternate, purely geometric approach to discretization based on shelling the high dimensional lattices.

2. DISCRETIZATION BASED ON STABILIZER THEORY

2.1. Stabilizers and the Generalized Pauli Matrices

We begin this section with some essential results from stabilizer theory. First, define the N-qubit Pauli group $\mathcal{G}_N$ as the set of all N-fold tensor products of 2×2 Pauli matrices, with four different overall phases to satisfy the closure requirement:

$$\mathcal{G}_N = \left\{\sigma_w, \sigma_x, \sigma_y, \sigma_z\right\}^{\otimes N} \otimes \{\pm 1, \pm i\},$$

where[6]

$$\sigma_w = \sigma_0 = \begin{bmatrix} 1 & 0 \\ 0 & 1 \end{bmatrix}, \quad \sigma_z = \sigma_1 = \begin{bmatrix} 1 & 0 \\ 0 & -1 \end{bmatrix},$$
$$\sigma_x = \sigma_2 = \begin{bmatrix} 0 & 1 \\ 1 & 0 \end{bmatrix}, \quad \sigma_y = \sigma_3 = \begin{bmatrix} 0 & -i \\ i & 0 \end{bmatrix}.$$

Clearly, each element of $\mathcal{G}_N$ acts on the N-qubit Hilbert space. $\mathcal{G}_N$ has order 4^{N+1}, and is generated by a minimal set of $2N$ elements, i.e. two non-identity σs acting on each qubit. We refer to individual elements of $\mathcal{G}_N$ as *generalized* Pauli matrices, and denote them $\Sigma_{\alpha\beta\ldots\zeta} = \sigma_\alpha \otimes \sigma_\beta \otimes \cdots \otimes \sigma_\zeta$. The generalized Pauli matrices share many of the properties of the 2×2 Pauli matrices. For example, they all either commute or anti-commute,

[5]Later, we will use the phrase rigorously, in reference to the information content of the discrete Hilbert space.

[6]The present numbering scheme has been chosen to coincide with the binary vector space representation of stabilizer codes, as in Ref. 8.

and

$$\begin{aligned}\Sigma_j^\dagger &= \Sigma_j \text{ (Hermitian)},\\ \Sigma_j^2 &= \text{id (Square root of unity)},\\ \mathrm{Tr}\Sigma_j^\dagger\Sigma_k &= 2^N\delta_{jk} \text{ (Orthogonal)}.\end{aligned}$$

A stabilizer is an Abelian subgroup of the Pauli group. In the present work, we are predominantly concerned with the commutation properties of the generalized Pauli matrices, so we neglect the phases $\{\pm 1, \pm i\}$ required for closure of $\mathcal{G}_N$ under multiplication. That is, we deal with the *set* $\mathcal{S}_N$ of 4^N generalized Pauli matrices rather than the group $\mathcal{G}_N$. To distinguish the Abelian subsets of $\mathcal{S}_N$ from the Abelian subgroups of $\mathcal{G}_N$, we refer to the former as *pseudo*stabilizers, a name which also highlights the close relationship between this work and stabilizer theory.

The largest possible subsets of $\mathcal{S}_N$ whose elements all mutually commute have 2^N elements. These *maximal* pseudostabilizers will form the foundation of our first discretization procedure.

2.2. The Uniform Hilbertian Polytope $\mathfrak{H}_N$

We are now in a position to discuss a formal definition for the uniform Hilbertian polytope for N qubits. First, we establish the desired properties the discrete sets must have. We seek to construct $\mathfrak{H}_N$ such that:

(1) It contains all the states $|b_0 b_1 \cdots b_{N-1}\rangle$ corresponding to the classical bit configurations.

(2) Each state of $\mathfrak{H}_N$ is geometrically equivalent to all the others (uniformity).

(3) The distance between two normalized states Ψ_j and Ψ_k, defined as

$$d_{jk} = 2\cos^{-1}(|\langle\Psi_j|\Psi_k\rangle|)$$

satisfies[7]

$$d_{jk} \geq \pi/2 \quad for\ all\ j,k.$$

(4) It is the largest set of states which satisfies the above requirements.

[7] Discretizations with a finer minimum distance may be useful and would be interesting to explore (for two qubits, see Section 3). For one qubit this could correspond, for instance, to the icosahedral geometry.

Denote by s_N^a the maximal pseudostabilizers in $\mathcal{S}_N$. Then these desired properties are obtained if we adopt the following construction for the vertices of $\mathfrak{H}_N$.

Definition 1. An N-qubit state vector is an element of $\mathfrak{H}_N$ if and only if it is a common eigenvector of each element of a *maximal* pseudostabilizer s_N^a. That is, if Σ_j is a generalized Pauli matrix on N qubits belonging to s_N^a, $|\Psi_j\rangle$ is an N-qubit state vector, and λ_j is an eigenvalue of Σ_j belonging to the vector $|\Psi_j\rangle$,

$$|\Psi_j\rangle \in \mathfrak{H}_N \Leftrightarrow \Sigma_j |\Psi_j\rangle = \lambda_j |\Psi_j\rangle \quad for\ all\ \Sigma_j \in s_N^a.$$

As a consequence of this definition, and from the theory of stabilizers, we find:

(a) Each s_N^a, which has $2^N - 1$ elements different from the identity, generates 2^N different discrete states all separated by $d_{jk} = \pi$. Each state corresponds to a unique pattern of $\lambda_j = \pm 1$.

(b) Each s_N^a shares exactly half, or 2^{N-1}, of its elements with its nearest neighbors; 2^{N-2} with its second-nearest neighbors, etc. Any discrete state in $\mathfrak{H}_N$ therefore has N "levels" of non-orthogonal neighboring states.

(c) For each s_N^a and each of its nearest neighbors s_N^b one can associate by a general algorithm a transformation from the common eigenvectors of s_N^a to those of s_N^b. That is, any two states of $\mathfrak{H}_N$ are linked by a finite sequence of similarity transformations.

(d) The similarity transformations are formed from generalized orthogonal $\pi/2$ rotations of the form:

$$X_{kl}^a = \frac{1}{\sqrt{2}} (\Sigma_k + i\Sigma_l), \text{ where } \Sigma_k, \Sigma_l \in s_N^a.$$

The superscript a denotes a subset s_N^a to which both its Σs belong and the subscripts specify the Σs. The inverse operations are:

$$(X_{kl}^a)^{-1} = \frac{1}{\sqrt{2}} (\Sigma_k - i\Sigma_l) = -i X_{lk}^a.$$

This definition implies that for any X,

$$X^\dagger X = \mathrm{id} \quad \text{(Unitary)},$$
$$X^4 = -\mathrm{id} \quad (\pi/2 \text{ Rotations}),$$

which is consistent with the property that a spin-1/2 acquires an overall phase of $e^{i\pi} = -1$ when rotated by 2π.

(e) The Xs generate the Clifford group $\mathcal{C}_N$, defined as the normalizer of the Pauli group[12], which has the property of leaving $\mathfrak{H}_N$ invariant (proof to follow).

(f) The set $\mathcal{S}_N$ of generalized Pauli matrices on N qubits contains

$$s = \prod_{k=0}^{N-1} (2^{N-k} + 1)$$

maximal pseudostabilizers s_N^a. Each has 2^N elements, and contributes 2^N simultaneous eigenvectors. The uniform Hilbertian polytope on N qubits $\mathfrak{H}_N$ therefore contains

$$V_N = 2^N \prod_{k=0}^{N-1} (2^{N-k} + 1)$$

vertices, or states[10]. The following table gives the first values of V_N, along with the number of classical bit configurations for comparison.

N	1	2	3	4	5	6	7
V_N	6	60	1080	36, 720	2, 423, 520	315, 057, 600	81, 284, 860, 800
C_N	2	4	8	16	32	64	128

The digital quantum information in N qubits can be defined as the information content of $\mathfrak{H}_N$, i.e., as $\log_2 V_N$. It is easy to show that V_N grows as $2^{(N^2+3N)/2}$, so this information content is super-extensive in N. While it is insufficient for algorithms which would be exponentially faster than classical ones, it is nonetheless a remarkable property for a discrete space.

We now turn to an explicit construction of the uniform Hilbertian polytope for the one- and two-qubit cases.

2.3. The One-qubit Case, $\mathfrak{H}_1$

We show here that $\mathfrak{H}_1$ is isomorphic to an octahedron. For one qubit, the set $\mathcal{S}_N$ is simply the Pauli matrices: $\mathcal{S}_1 = \{\sigma_w, \sigma_x, \sigma_y, \sigma_z\}$. The last three σs anti-commute with one another, while they all commute with the identity σ_w. So the three sets of mutually commuting matrices are trivial to construct: $s_1^1 = \{\sigma_w, \sigma_z\}$, $s_1^2 = \{\sigma_w, \sigma_x\}$ and $s_1^3 = \{\sigma_w, \sigma_y\}$.

When the elements of s_1^1 are diagonalized, we obtain the computational basis:

$$|+z\rangle = |0\rangle\,,$$
$$|-z\rangle = |1\rangle\,.$$

s_1^2 generates the pair

$$|+x\rangle = \frac{|0\rangle + |1\rangle}{\sqrt{2}},$$
$$|-x\rangle = \frac{|0\rangle - |1\rangle}{\sqrt{2}}.$$

And s_1^3 generates

$$|+y\rangle = \frac{|0\rangle + i\,|1\rangle}{\sqrt{2}},$$
$$|-y\rangle = \frac{|0\rangle - i\,|1\rangle}{\sqrt{2}}.$$

There are three orthogonal $\pi/2$ rotations, which form the *seed* of $\mathfrak{H}_1$:

$$X_{0\,1}^1 = \tfrac{1}{\sqrt{2}}\,(\sigma_0 + i\sigma_1)\,,$$
$$X_{0\,2}^2 = \tfrac{1}{\sqrt{2}}\,(\sigma_0 + i\sigma_2)\,,$$
$$X_{0\,3}^3 = \tfrac{1}{\sqrt{2}}\,(\sigma_0 + i\sigma_3)\,.$$

The diagonalization of the seed elements leads directly to the six eigenstates, as summarized in the table below. The states are listed here as unnormalized row vectors for clarity, and are separated into columns according to their eigenvalues.

Set	$1+i$	$1-i$
1	$(1, 0)$	$(0, 1)$
2	$(1, 1)$	$(1, -1)$
3	$(1, i)$	$(1, -i)$

Each of the $\pi/2$ rotations has an inverse:

$$(X_{0\,k}^k)^{-1} = -i\,X_{k\,0}^k = \frac{1}{\sqrt{2}}\,(\sigma_0 - i\sigma_k)\,.$$

It is easy to verify that

$$(X_{0k}^k)^2 = \tfrac{1}{2}(\sigma_0 + i\sigma_k)^2 = i\sigma_k$$

and that the Xs are mapped into one another by similarity transformation:

$$\begin{aligned} X_{0\,j}^{j} X_{0i}^{i} \left(X_{0\,j}^{j}\right)^{-1} &= \frac{1}{2\sqrt{2}}(\sigma_0 + i\sigma_j)(\sigma_0 + i\sigma_i)(\sigma_0 - i\sigma_j) \\ &= \frac{1}{2\sqrt{2}}\left(2\sigma_0 + 2i\ \epsilon_{ijk}\sigma_k\right) \\ &= X_{0k}^k \quad \text{if} \quad \epsilon_{ijk} = 1 \\ &= \left(X_{0k}^k\right)^{-1} \quad \text{if} \quad \epsilon_{ijk} = -1 \end{aligned}$$

This implies that each X transforms a member of $\mathfrak{H}_1$ into its neighbor.

Proof. If

$$X^j \left|\Psi_j\right\rangle = \lambda_j \left|\Psi_j\right\rangle$$

and if

$$\left|\Psi_{i(j)}\right\rangle = X^i \left|\Psi_j\right\rangle,$$

then

$$\begin{aligned} X^i X^j (X^i)^{-1} \left|\Psi_{i(j)}\right\rangle &= X^i X^j \left|\Psi_j\right\rangle \\ &= \lambda_j X^i \left|\Psi_j\right\rangle \\ &= \lambda_j \left|\Psi_{i(j)}\right\rangle \end{aligned}$$

therefore $\left|\Psi_{i(j)}\right\rangle$ is an eigenvector of X^k. □

The Xs with their inverse generate a 24 element group isomorphic to the octahedral group of pure rotations which leaves the octahedron invariant.

2.4. The Two-qubit Case, $\mathfrak{H}_2$

The set of generalized Pauli matrices for two qubits $\mathcal{S}_2$ comprises $4^2 = 16$, $2^2 \times 2^2$ matrices given by $\Sigma_{\lambda\mu} = \sigma_\lambda \otimes \sigma_\mu$, $\lambda, \mu = w, x, y, z$, as presented below. We write the index on the σs in binary, then concatenate the two strings to form the new index for the Σs. For example, $\sigma_y \otimes \sigma_z = \sigma_3 \otimes \sigma_1 = \sigma_{11} \otimes \sigma_{01} = \Sigma_{1101} = \Sigma_{13}$ (Figure 1).

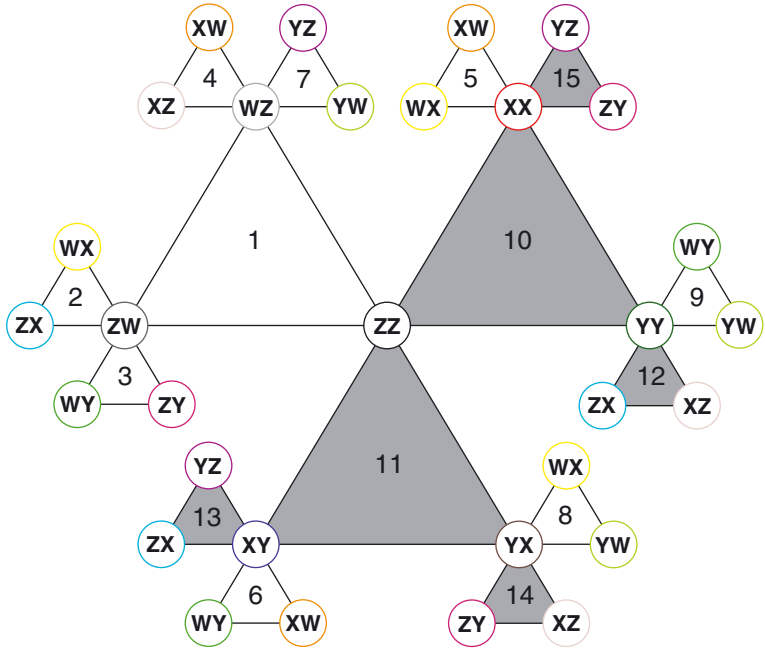

Fig. 1. Graph of the set $\mathcal{S}_2$ of two-qubit generalized Pauli matrices Σ_j (circles bearing the subscript of the matrix in letter notation) and by the pseudostabilizers (triangles formed by three connected circles). The three Σs in a triangle share four common eigenvectors which form an orthonormal basis spanning the two-qubit Hilbert space. The 15 triangles thus give 15 sets of four basis vectors. Shaded triangles correspond to entangled states while non-shaded triangles correspond to product states. Neighboring triangles have one (non-identity) Σ in common, and each (non-identity) Σ is shared by three triangles. The line segments joining the vertices of a triangle correspond to pairs $\{j,k\}$ of commuting matrices; each segment therefore specifies a $\pi/2$ rotation $X_{j,k}=(\Sigma_j+i\Sigma_k)/\sqrt{2}$ that transforms the eigenvectors of an adjacent triangle into its neighbor. The figure thus constitutes a "road map" for navigating the discrete set $\mathfrak{H}_2$. (Repeated circles indicate the closure of the graph.)

$$\Sigma_{ww}=\Sigma_0=\begin{bmatrix}1&0&0&0\\0&1&0&0\\0&0&1&0\\0&0&0&1\end{bmatrix}\qquad \Sigma_{wz}=\Sigma_1=\begin{bmatrix}1&0&0&0\\0&-1&0&0\\0&0&1&0\\0&0&0&-1\end{bmatrix}$$

$$\Sigma_{wx}=\Sigma_2=\begin{bmatrix}0&1&0&0\\1&0&0&0\\0&0&0&1\\0&0&1&0\end{bmatrix}\qquad \Sigma_{wy}=\Sigma_3=\begin{bmatrix}0&-i&0&0\\i&0&0&0\\0&0&0&-i\\0&0&i&0\end{bmatrix}$$

$$\Sigma_{zw}=\Sigma_4=\begin{bmatrix}1&0&0&0\\0&1&0&0\\0&0&-1&0\\0&0&0&-1\end{bmatrix} \qquad \Sigma_{zz}=\Sigma_5=\begin{bmatrix}1&0&0&0\\0&-1&0&0\\0&0&-1&0\\0&0&0&1\end{bmatrix}$$

$$\Sigma_{zx}=\Sigma_6=\begin{bmatrix}0&1&0&0\\1&0&0&0\\0&0&0&-1\\0&0&-1&0\end{bmatrix} \qquad \Sigma_{zy}=\Sigma_7=\begin{bmatrix}0&-i&0&0\\i&0&0&0\\0&0&0&i\\0&0&-i&0\end{bmatrix}$$

$$\Sigma_{xw}=\Sigma_8=\begin{bmatrix}0&0&1&0\\0&0&0&1\\1&0&0&0\\0&1&0&0\end{bmatrix} \qquad \Sigma_{xz}=\Sigma_9=\begin{bmatrix}0&0&1&0\\0&0&0&-1\\1&0&0&0\\0&-1&0&0\end{bmatrix}$$

$$\Sigma_{xx}=\Sigma_{10}=\begin{bmatrix}0&0&0&1\\0&0&1&0\\0&1&0&0\\1&0&0&0\end{bmatrix} \qquad \Sigma_{xy}=\Sigma_{11}=\begin{bmatrix}0&0&0&-i\\0&0&i&0\\0&-i&0&0\\i&0&0&0\end{bmatrix}$$

$$\Sigma_{yw}=\Sigma_{12}=\begin{bmatrix}0&0&-i&0\\0&0&0&-i\\i&0&0&0\\0&i&0&0\end{bmatrix} \qquad \Sigma_{yz}=\Sigma_{13}=\begin{bmatrix}0&0&-i&0\\0&0&0&i\\i&0&0&0\\0&-i&0&0\end{bmatrix}$$

$$\Sigma_{yx}=\Sigma_{14}=\begin{bmatrix}0&0&0&-i\\0&0&-i&0\\0&i&0&0\\i&0&0&0\end{bmatrix} \qquad \Sigma_{yy}=\Sigma_{15}=\begin{bmatrix}0&0&0&-1\\0&0&1&0\\0&1&0&0\\-1&0&0&0\end{bmatrix}$$

The products of these matrices can easily be found from

$$\Sigma_{\lambda\mu}\Sigma_{\eta\nu}=\left(\sigma_\lambda\otimes\sigma_\mu\right)\left(\sigma_\eta\otimes\sigma_\nu\right)=\left(\sigma_\lambda\sigma_\eta\right)\otimes\left(\sigma_\mu\sigma_\nu\right).$$

The maximal pseudostabilizers in $\mathcal{S}_2$ are presented below.[8]

Each of these 15 sets, or pseudostabilizers, will yield four simultaneous eigenvectors, contributing four states to $\mathfrak{H}_2$. We therefore recover the result that $\mathfrak{H}_2$ has 60 states.

[8]Constructing the subsets of mutually commuting Pauli matrices can be done through a series of logical steps. The key is to note that $[\Sigma_{jk},\Sigma_{lm}]=0$ requires either $[\sigma_j,\sigma_l]=[\sigma_k,\sigma_m]=0$ or $\{\sigma_j,\sigma_l\}=\{\sigma_k,\sigma_m\}=0$

Subset #	Letter notation	Number notation
1	$\{\Sigma_{ww}, \Sigma_{wz}, \Sigma_{zw}, \Sigma_{zz}\}$	$\{\Sigma_0, \Sigma_1, \Sigma_4, \Sigma_5\}$
2	$\{\Sigma_{ww}, \Sigma_{wx}, \Sigma_{zw}, \Sigma_{zx}\}$	$\{\Sigma_0, \Sigma_2, \Sigma_4, \Sigma_6\}$
3	$\{\Sigma_{ww}, \Sigma_{wy}, \Sigma_{zw}, \Sigma_{zy}\}$	$\{\Sigma_0, \Sigma_3, \Sigma_4, \Sigma_7\}$
4	$\{\Sigma_{ww}, \Sigma_{wz}, \Sigma_{xw}, \Sigma_{xz}\}$	$\{\Sigma_0, \Sigma_1, \Sigma_8, \Sigma_9\}$
5	$\{\Sigma_{ww}, \Sigma_{wx}, \Sigma_{xw}, \Sigma_{xx}\}$	$\{\Sigma_0, \Sigma_2, \Sigma_8, \Sigma_{10}\}$
6	$\{\Sigma_{ww}, \Sigma_{wy}, \Sigma_{xw}, \Sigma_{xy}\}$	$\{\Sigma_0, \Sigma_3, \Sigma_8, \Sigma_{11}\}$
7	$\{\Sigma_{ww}, \Sigma_{wz}, \Sigma_{yw}, \Sigma_{yz}\}$	$\{\Sigma_0, \Sigma_1, \Sigma_{12}, \Sigma_{13}\}$
8	$\{\Sigma_{ww}, \Sigma_{wx}, \Sigma_{yw}, \Sigma_{yx}\}$	$\{\Sigma_0, \Sigma_2, \Sigma_{12}, \Sigma_{14}\}$
9	$\{\Sigma_{ww}, \Sigma_{wy}, \Sigma_{yw}, \Sigma_{yy}\}$	$\{\Sigma_0, \Sigma_3, \Sigma_{12}, \Sigma_{15}\}$
10*	$\{\Sigma_{ww}, \Sigma_{zz}, \Sigma_{xx}, \Sigma_{yy}\}$	$\{\Sigma_0, \Sigma_5, \Sigma_{10}, \Sigma_{15}\}$
11*	$\{\Sigma_{ww}, \Sigma_{zz}, \Sigma_{xy}, \Sigma_{yx}\}$	$\{\Sigma_0, \Sigma_5, \Sigma_{11}, \Sigma_{14}\}$
12*	$\{\Sigma_{ww}, \Sigma_{zx}, \Sigma_{xz}, \Sigma_{yy}\}$	$\{\Sigma_0, \Sigma_6, \Sigma_9, \Sigma_{15}\}$
13*	$\{\Sigma_{ww}, \Sigma_{zx}, \Sigma_{xy}, \Sigma_{yz}\}$	$\{\Sigma_0, \Sigma_6, \Sigma_{11}, \Sigma_{13}\}$
14*	$\{\Sigma_{ww}, \Sigma_{zy}, \Sigma_{xz}, \Sigma_{yx}\}$	$\{\Sigma_0, \Sigma_7, \Sigma_9, \Sigma_{14}\}$
15*	$\{\Sigma_{ww}, \Sigma_{zy}, \Sigma_{xx}, \Sigma_{yz}\}$	$\{\Sigma_0, \Sigma_7, \Sigma_{10}, \Sigma_{13}\}$

These subsets can be classified as corresponding to entangled or product states by examining their generators. Note that each pseudostabilizer is generated by any two of its non-identity elements. The presence of the one-qubit identity σ_w when the generators are decomposed into tensor products of one-qubit Pauli matrices implies that the states corresponding to that subset are product states. Conversely, the absence of the identity in this decomposition indicates that the states corresponding to that Abelian subset are fully entangled states. The subsets whose generators do not contain the one-qubit identity are denoted here and below by an asterisk.

We can obtain all the states of $\mathfrak{H}_2$ directly by forming a mixed linear combination of the first two non-identity elements from within each set. For instance $X_{3,12} = (1/\sqrt{2})(\Sigma_{wy} + i\Sigma_{yw})$, when diagonalized, gives four orthogonal eigenvectors with four different eigenvalues. (Note that other rotations from s_2^1, such as $X_{12,15} = (1/\sqrt{2})(\Sigma_{12} + i\Sigma_{15})$ and $X_{3,15} = (1/\sqrt{2})(\Sigma_3 + i\Sigma_{15})$ will produce the same four eigenvectors, but with permuted eigenvalues.) We thus construct in this manner 15 generalized Xs, each having a different principal axis, which form the seed of $\mathfrak{H}_2$. Diagonalization of the seed Xs exhaustively gives the eigenvectors constituting $\mathfrak{H}_2$. We list these eigenvectors below, separated into columns corresponding to the eigenvalues $(\pm 1 \ \pm i)$. For clarity, we list them as unnormalized row vectors. Again, entangled states are denoted by an asterisk on the set label.

Set	$-1-i$	$-1+i$	$1-i$	$1+i$
1	$(0,0,0,1)$	$(0,1,0,0)$	$(0,0,1,0)$	$(1,0,0,0)$
2	$(0,0,-1,1)$	$(-1,1,0,0)$	$(0,0,1,1)$	$(1,1,0,0)$
3	$(0,0,i,1)$	$(i,1,0,0)$	$(0,0,-i,1)$	$(-i,1,0,0)$
4	$(0,-1,0,1)$	$(0,1,0,1)$	$(-1,0,1,0)$	$(1,0,1,0)$
5	$(1,-1,-1,1)$	$(-1,1,-1,1)$	$(-1,-1,1,1)$	$(1,1,1,1)$
6	$(-i,-1,i,1)$	$(i,1,i,1)$	$(i,-1,-i,1)$	$(-i,1,-i,1)$
7	$(0,i,0,1)$	$(0,-i,0,1)$	$(i,0,1,0)$	$(-i,0,1,0)$
8	$(-i,i,-1,1)$	$(i,-i,-1,1)$	$(i,i,1,1)$	$(-i,-i,1,1)$
9	$(-1,i,i,1)$	$(1,-i,i,1)$	$(1,i,-i,1)$	$(1,i,i,-1)$
10*	$(0,-1,1,0)$	$(-1,0,0,1)$	$(1,0,0,1)$	$(0,1,1,0)$
11*	$(i,0,0,1)$	$(0,-i,1,0)$	$(0,i,1,0)$	$(-i,0,0,1)$
12*	$(1,1,-1,1)$	$(-1,1,1,1)$	$(1,-1,1,1)$	$(1,1,1,-1)$
13*	$(i,-i,1,1)$	$(i,i,-1,1)$	$(i,i,1,-1)$	$(-i,i,1,1)$
14*	$(i,1,-i,1)$	$(-i,1,i,1)$	$(i,-1,i,1)$	$(i,1,i,-1)$
15*	$(-1,-i,i,1)$	$(-1,i,-i,1)$	$(1,-i,-i,1)$	$(1,i,i,1)$

Note that the first stabilizer of the product sector corresponds to the computational basis, while the first stabilizer of the entangled sector corresponds to the Bell basis.

This method not only finds the states of $\mathfrak{H}_2$ in an exhaustive way. It also provides a road map for navigating the discrete set. To illustrate this, consider three pseudostabilizers which we call s^a, s^b and s^c. They have two generalized Pauli matrices in common, one of them being the trivial Σ_0. We chose one of the two and call it Σ_m. Consider three $\Sigma \neq \Sigma_m$,

$$\Sigma_j \in s^a, \quad \Sigma_k \in s^b, \quad \Sigma_l \in s^c$$

such that

$$\{\Sigma_j, \Sigma_k\} = \{\Sigma_k, \Sigma_l\} = \{\Sigma_l, \Sigma_j\} = 0.$$

Since all pairs of generalized Pauli matrices that do not commute must anti-commute, they also satisfy

$$[\Sigma_j, \Sigma_m] = [\Sigma_k, \Sigma_m] = [\Sigma_l, \Sigma_m] = 0.$$

Then, it is easy to show by a direct calculation that

$$X^a_{m\,j} = \tfrac{1}{\sqrt{2}}\left(\Sigma_m + i\,\Sigma_j\right),$$
$$X^b_{m\,k} = \tfrac{1}{\sqrt{2}}\left(\Sigma_m + i\,\Sigma_k\right),$$
$$X^c_{m\,l} = \tfrac{1}{\sqrt{2}}\left(\Sigma_m + i\,\Sigma_l\right),$$

have one of the properties:

$$X^b_{m\,k} X^a_{m\,j} X^b_{k\,m} = X^c_{m\,l}$$

or

$$X^b_{m\,k} X^a_{m\,j} X^b_{k\,m} = (X^c_{m\,l})^{-1} = -i\,X^c_{l\,m}$$

depending on whether the two anti-commuting σs in the decomposition of $\Sigma_j \Sigma_k$ appear in cyclic order or anti-cyclic order, respectively. This means, following the proof given for the one-qubit case, that all the eigenvectors of s^a are transformed into the eigenvectors of s^c by the transformation X^b.

Altogether, there are 120 different generalized two-qubit $\pi/2$ rotations generated by the scheme

$$X_{i\,j} = \frac{1}{\sqrt{2}}\left(\Sigma_i + i\,\Sigma_j\right),$$

where Σ_i and Σ_j commute.

Among these Xs, there is a subset that plays an important practical role. These are $\pi/2$ rotations of the form

$$X_{0\,j} = \frac{1}{\sqrt{2}}\left(\Sigma_0 + i\,\Sigma_j\right).$$

They correspond to the unitary time-evolution operator

$$U(t) = e^{i\,\Sigma_j \tau}$$

with $\tau = \pi/4$, and are thus directly implemented by a Hamiltonian proportional to Σ_j. These rotations constitute the practical means of navigating $\mathfrak{H}_2$. They can be seen as the "primitives" of the Clifford group, as we show below.

But first, it is important to note that the generalized Pauli matrices in the above arguments are not limited to the two-qubit case, but can in fact be over any number of qubits. These results are therefore directly generalizable to larger Hilbert spaces H_N and larger discrete sets $\mathfrak{H}_N$. We duly conclude that our generalized $\pi/2$ rotations on N qubits, constructed from the pseudostabilizers s^a_N, leave $\mathfrak{H}_N$ invariant.

2.5. The Generalized $\pi/2$ Rotations Generate the N-qubit Clifford Group

So far we have successfully discretized the continuous Hilbert space H_N, and in doing so we have described a class of generalized $\pi/2$ rotations that leave the $\mathfrak{H}_N$ invariant. From the point of view of operators acting in H_N, this discretization means we have reduced the continuous transformation group $SU(2^N)$ to a finite group. Here we show that this finite group is the N-qubit Clifford group $\mathcal{C}_N$.

The Clifford group is defined as the normalizer of the Pauli group. That is, a unitary operator X is contained in $\mathcal{C}_N$ if and only if

$$X \Sigma X^{-1} \in \mathcal{G}_N \quad \forall \ \Sigma \in \mathcal{G}_N.$$

First, let us show that our Xs are elements of $\mathcal{C}_N$. That is,

$$X_{jk} = \frac{1}{\sqrt{2}}(\Sigma_j + i\Sigma_k) \in \mathcal{C}_N \ \text{ if } \ [\Sigma_j, \Sigma_k] = 0.$$

We have

$$\begin{aligned} \Sigma_j \Sigma_l &= \varepsilon_{jl} \Sigma_l \Sigma_j, \\ \Sigma_k \Sigma_l &= \varepsilon_{kl} \Sigma_l \Sigma_k, \end{aligned}$$

where $\varepsilon_{jl} = \pm 1$ and $\varepsilon_{kl} = \pm 1$.Thus,

$$\begin{aligned} X_{jk} \Sigma_l X_{jk}^{-1} &= \tfrac{1}{2} (\Sigma_j + i\Sigma_k) \Sigma_l (\Sigma_j - i\Sigma_k) \\ &= \tfrac{1}{2} \Sigma_l (\varepsilon_{jl} \Sigma_j + i\varepsilon_{kl} \Sigma_k)(\Sigma_j - i\Sigma_k) \\ &= \tfrac{1}{2} \varepsilon_{jl} \Sigma_l (\Sigma_j + i\varepsilon_{kl}\varepsilon_{jl} \Sigma_k)(\Sigma_j - i\Sigma_k). \end{aligned}$$

If $\varepsilon_{kl}\varepsilon_{jl} = 1$,

$$\begin{aligned} &= \tfrac{1}{2} \varepsilon_{jl} \Sigma_l (2\Sigma_0 + i\Sigma_k \Sigma_j - i\Sigma_j \Sigma_k) \\ &= \varepsilon_{jl} \Sigma_l \in \mathcal{G}_N. \end{aligned}$$

If $\varepsilon_{kl}\varepsilon_{jl} = -1$,

$$\begin{aligned} &= \tfrac{1}{2} \varepsilon_{jl} \Sigma_l (-i\Sigma_k \Sigma_j - i\Sigma_j \Sigma_k) \\ &= -i\varepsilon_{jl} \Sigma_l \Sigma_j \Sigma_k \in \mathcal{G}_N. \end{aligned}$$

So the generalized $\pi/2$ rotations on N qubits are elements of the Clifford group.

Now note that the Clifford group is generated by the Hadamard,

$$\mathrm{H} = \frac{1}{\sqrt{2}} \begin{bmatrix} 1 & 1 \\ 1 & -1 \end{bmatrix}$$

phase,

$$\mathrm{S} = \begin{bmatrix} 1+i & 0 \\ 0 & 1-i \end{bmatrix}$$

and CNOT,

$$\mathrm{CNOT} = \begin{bmatrix} 1&0&0&0 \\ 0&1&0&0 \\ 0&0&0&1 \\ 0&0&1&0 \end{bmatrix}$$

gates[5]. The Hadamard gate may be composed from the one-qubit $\pi/2$ rotations X_{02} and X_{01}:

$$\begin{aligned} \mathrm{H} &= X_{02}X_{01}(X_{20})^{-1} \\ &= -iX_{02}X_{01}X_{02} \\ &= \frac{-i}{2\sqrt{2}} \begin{bmatrix} 1 & i \\ i & 1 \end{bmatrix} \begin{bmatrix} 1+i & 0 \\ 0 & 1-i \end{bmatrix} \begin{bmatrix} 1 & i \\ i & 1 \end{bmatrix} \\ &= \frac{1}{\sqrt{2}} \begin{bmatrix} 1 & 1 \\ 1 & -1 \end{bmatrix}. \end{aligned}$$

The phase gate may be trivially constructed from a single one-qubit $\pi/2$ rotation:

$$\begin{aligned} \mathrm{S} &= X_{01} \\ &= \begin{bmatrix} 1+i & 0 \\ 0 & 1-i \end{bmatrix}, \end{aligned}$$

while the CNOT is simply the product of three Xs:

$$\begin{aligned} \mathrm{CNOT} &= (X_{02})^{-1}X_{06}(X_{04})^{-1} \\ &= -X_{20}X_{06}X_{40} \\ &= \frac{-1}{2\sqrt{2}} \begin{bmatrix} i&1&0&0 \\ 1&i&0&0 \\ 0&0&i&1 \\ 0&0&1&i \end{bmatrix} \begin{bmatrix} 1&i&0&0 \\ i&1&0&0 \\ 0&0&1&-i \\ 0&0&-i&1 \end{bmatrix} \begin{bmatrix} 1+i&0&0&0 \\ 0&1+i&0&0 \\ 0&0&-1+i&0 \\ 0&0&0&-1+i \end{bmatrix} \\ &= \frac{1}{\sqrt{2}} \begin{bmatrix} 1-i&0&0&0 \\ 0&1-i&0&0 \\ 0&0&0&1-i \\ 0&0&1-i&0 \end{bmatrix}. \end{aligned}$$

So our generalized $\pi/2$ rotations allow a direct construction of a gate set that generates the Clifford group. The finite transformation group leaving

$\mathfrak{H}_N$ invariant, generated by the generalized $\pi/2$ rotations on N qubits, is thus the N-qubit Clifford group $\mathcal{C}_N$.

2.6. Comments

One of the motives we presented for this work was the difficulty we anticipate in achieving the reliability requisite for fault-tolerant quantum computation. Clearly, limiting the register to a finite number of possible states must alleviate this difficulty, but by how much?

It can be derived from the properties of the Pauli group that each pseudostabilizer s_N^a has N levels of non-orthogonal neighbors. Since the eigenstates of neighboring pseudostabilizers are connected by a single $\pi/2$ rotation, any state on $\mathfrak{H}_N$ can be reached from any other in at most $N+1$ such rotations. This is to be compared with the result that an arbitrary state in the full Hilbert space can be reached to within an error ϵ by concatenating $\mathcal{O}(\log^c(1/\epsilon))$ rotations from a universal set, with $c \approx 2$. In addition, note that the CNOT and H gates are not directly implemented by a physical Hamiltonian, but must be built up from $\pi/2$ rotations which are naturally realized with accessible field variations, so there is a second simplification from working with the $\pi/2$ rotations rather than standard universal gate sets such as {H, S, T, CNOT}.

From an experimentalist's point of view, therefore, the Xs form a very natural language for building quantum gates. A rotation of the form $X_{0\ j} = (\Sigma_0 + i\Sigma_j)/\sqrt{2}$ is directly implemented by a term in the Hamiltonian proportional to Σ_j. And as shown above, this class of rotations generates $\mathcal{C}_N$. The Xs are thus the basic instructions for a sort of "machine language" for quantum processors. The following section shows a simple example of their calculus.

2.7. Sample Application of Digital Quantum Information: Implementing CNOT

The Hamiltonian describing a given physical system determines which of the generalized $\pi/2$ rotations will be directly realizable in that system. Implementing CNOT according to the decomposition in Section 2.5 requires a physical system with a Hamiltonian proportional to Σ_{zx} in order to realize the entangling operation $X_{0\,6} = (\Sigma_{ww} + i\Sigma_{zx})/\sqrt{2}$. Though this type of inter-qubit interaction is possible[9], most qubit systems rely on a less exotic interaction, such as one proportional to Σ_{zz} or Σ_{xx}. How can we implement the CNOT gate in one of these more standard registers?

[9] As a charge-flux coupling between superconducting qubits, for example.

Specifically, suppose the system is described by a two-qubit Hamiltonian of the form

$$H = a(t)\Sigma_1 + b(t)\Sigma_2 + c(t)\Sigma_4 + d(t)\Sigma_8 + e(t)\Sigma_5,$$

where the tuning parameters a, b, c, d, e allow the relative strengths of the terms to be adjusted during an experiment. Our task is to replace the rotation $X_{0\,6}$ in the sequence $(X_{0\,2})^{-1}X_{0\,6}(X_{0\,4})^{-1}$ with a rotation or sequence of rotations generated by the above Hamiltonian. Following the discussion in Sections 2.3 and 2.4 on the relationships between the generalized $\pi/2$ rotations, it is straightforward to calculate that $X_{0\,6} = (X_{0\,3})^{-1}X_{0\,5}X_{0\,3}$ while $X_{0\,3} = (X_{0\,1})^{-1}X_{0\,2}X_{0\,1}$. Together these give an alternate decomposition that employs only directly realizable Xs :

$$\begin{aligned}\text{CNOT} &= (X_{0\,2})^{-1}X_{0\,6}(X_{0\,4})^{-1} \\ &= (X_{0\,2})^{-1}(X_{0\,3})^{-1}X_{0\,5}X_{0\,3}(X_{0\,4})^{-1} \\ &= (X_{0\,2})^{-1}X_{0\,1}X_{0\,2}(X_{0\,1})^{-1}X_{0\,5}(X_{0\,1})^{-1}X_{0\,2}X_{0\,1}(X_{0\,4})^{-1}.\end{aligned}$$

Since the decompositions differ in their implementation but not in their meaning, such sequences are "synonyms". It is important to note that the CNOT is not a special case: a synonym suitable for a particular implementation could likewise be calculated for *any* gate in C_2.

2.8. Conclusion to Section 2

In this section we have presented a geometric method for producing from the continuous Hilbert space H_N a discrete, uniform sampling $\mathfrak{H}_N$. Because all the states in the discrete set are geometrically equivalent, $\mathfrak{H}_N$ represents a generalized Platonic solid in H_N. This method is closely related to the stabilizer formalism of quantum error-correcting codes. Inherent in our construction is a description of how different elements of $\mathfrak{H}_N$ are related by transformations generated by physical Hamiltonians expressed in the basis of generalized Pauli matrices. This has been demonstrated in detail for $\mathfrak{H}_1$ and $\mathfrak{H}_2$, and is obtainable by direct analogy for higher-dimensional spaces. These ideas provide a useful tool for analyzing problems in traditional quantum computation, as the example above illustrates. And though computation over the discrete set $\mathfrak{H}_N$ is clearly less powerful than computation in the full H_N, it is potentially more powerful than classical computation.

3. AN ALTERNATE APPROACH TO DISCRETIZATION: SHELLING THE HIGH-DIMENSIONAL DENSE LATTICES

In this last section, we present an alternate approach to discretization that addresses the Hilbert space directly, without reference to operators in H_N or the relevant transformation groups.

Our strategy here is the following (we note $n = 2^N$): the normalization condition, together with the writing of complex numbers as pairs of real numbers, identifies the Hilbert space H_N to the high-dimensional sphere S^{2n-1} embedded in $\mathbb{R}^{2n}$. In order to discretize these hyperspheres, we use the successive shells of dense lattices in $\mathbb{R}^{2n}$. At the same time, we must take into account the global phase freedom, and show how a discretization of the projective Hilbert space is induced. This means that several points on S^{2n-1} will represent the same physical state, as explained below. In light of this, it is important to distinguish between "qubit states"—the quantum states associated to the points on S^{2n-1}—and "physical states"—the states in the projective Hilbert space, which has the geometry of a complex projective space CP^{n-1}.

As in Section 2, we again focus on the one- and two-qubit cases. The discretization of H_1 is first presented in terms of the 24 vertices of a self-dual polytope on S^3, denoted $\{3, 4, 3\}$, which is the first shell of the densest packing in $\mathbb{R}^4$, denoted Λ_4. These 24 vertices correspond to 24 one-qubit states, and, modulo a global phase, to six physical states. For the two-qubit case, we use the *Gosset polytope*, the first shell of the densest packing in $\mathbb{R}^8$, denoted E_8. We find that this polytope has 240 vertices corresponding to 240 two-qubit states, which leads to 60 physical states: 36 separable states and 24 maximally entangled states, just as in Section 2.

The N-qubit Hilbert space is high-dimensional, and its multipartite nature (it is the tensor product of single-qubit Hilbert space) induces a subtle structure related to the state's various levels of entanglement [13,14], which is not fully understood for $N \geq 3$. The Hopf map that is used here in the two-qubit case is entanglement-sensitive, which translates here in grouping sets of equally entangled qubit states.

3.1. The One-qubit Case

The generic one-qubit state reads

$$|\Psi\rangle = t_0 |0\rangle + t_1 |1\rangle ,$$

with $|t_0|^2 + |t_1|^2 = 1$. The normalization condition identifies the set of normalized states to a sphere S^3 embedded in $\mathbb{R}^4$. The projective case—the set

of states modulo a global phase—leads to the Bloch sphere description, which can be seen as the base of the S^3 Hopf fibration,[15,16]. An interesting discrete model on S^3 is provided by the self-dual $\{3, 4, 3\}$ polytope[17]. It is related to the "Hurwitz" quaternion group. We now give two possible (dual) coordinates for its vertices, in each case as a real quadruplet and a complex pair. The correspondence between real quadruplets and complex pairs amounts simply to taking the first two (last two) real numbers as the real and imaginary part of the first (second) complex number. The first (second) complex number in the pair corresponds to t_0 (t_1).

A first set, denoted T_1, is the union of the eight permutations of type $(\pm 1, 0, 0, 0)$ and the 16 permutations of type $(1/2)(\pm 1, \pm 1, \pm 1, \pm 1)$. Note that, modulo a global phase factor, these 24 points really represent six different physical states, which appear on the Bloch sphere as opposite points on the three orthogonal axes x, y, z. Indeed, the four points,

Real quadruplets	Complex pairs
$(1, 0, 0, 0)$	$(1, 0)$
$(-1, 0, 0, 0)$	$(-1, 0)$
$(0, 1, 0, 0)$	$(i, 0)$
$(0, -1, 0, 0)$	$(-i, 0)$

represent the states $|\Psi_1, \omega\rangle = e^{i\omega}|0\rangle$, with $\omega = 0, \pi/2, \pi, 3\pi/2$, which map to the same point on the Bloch sphere (the north pole), and they are therefore associated to the physical state $|\Psi_1\rangle$. Equivalently, the four points

Real quadruplets	Complex pairs
$(0, 0, 1, 0)$	$(0, 1)$
$(0, 0, -1, 0)$	$(0, -1)$
$(0, 0, 0, 1)$	$(0, i)$
$(0, 0, 0, -1)$	$(0, -i)$

represent the four states $|\Psi_2, \omega\rangle = e^{i\omega}|1\rangle$ with $\omega = 0, \pi/2, \pi, 3\pi/2$. The other 16 vertices represent four other physical states, in the following way:

$$|\Psi_3\rangle \equiv \frac{e^{i(\omega+\pi/4)}}{\sqrt{2}}(|0\rangle - |1\rangle), \qquad |\Psi_4\rangle \equiv \frac{e^{i(\omega+\pi/4)}}{\sqrt{2}}(|0\rangle - |1\rangle),$$
$$|\Psi_5\rangle \equiv \frac{e^{i(\omega+\pi/4)}}{\sqrt{2}}(|0\rangle + i\,|1\rangle), \qquad |\Psi_6\rangle \equiv \frac{e^{i(\omega+\pi/4)}}{\sqrt{2}}(|0\rangle - i\,|1\rangle),$$

with $\omega = 0, \pi/2, \pi, 3\pi/2$.

For the later purpose of a discrete two-qubit construction, it is useful to describe a second version of the polytope $\{3, 4, 3\}$, for which the 24 vertices form a set T_2 given by 24 permutations of the type $\{\pm 1, \pm 1, 0, 0\}/\sqrt{2}$. This polytope is obtained from the former one through a *screw* motion on $S^3$of angle $\pi/4$. This set leads to 24 states

$$|\Phi_l, \omega\rangle = \epsilon\,|\Psi_l, \omega\rangle, \quad l = 1, \ldots, 6, \ \omega = 0, \pi/2, \pi, 3\pi/2, \text{ and } \epsilon = e^{i\pi/4}$$

and to the six one-qubit physical states $|\Phi_l\rangle$ identical to $|\Psi_l\rangle$. Indeed, the six states $|\Psi_j\rangle$ sit at the vertices of a regular octahedron. Since the states $|\Phi_l, \omega\rangle$ only differ from $|\Psi_l, \omega\rangle$ by a global phase, they map onto the same six points on the Bloch sphere.

3.2. The Two-qubit Case

We now consider the two-qubit case, for which a generic state reads:

$$|\Psi\rangle = t_{00}\,|00\rangle + t_{01}\,|01\rangle + t_{10}\,|10\rangle + t_{11}\,|11\rangle, \quad \text{and}$$
$$|t_{00}|^2 + |t_{01}|^2 + |t_{10}|^2 + |t_{11}|^2 = 1.$$

The normalization condition identifies the set of normalized states to the sphere S^7 embedded in $\mathbb{R}^8$.

As for the one-qubit case, we consider the first shell of points in the densest lattice in $\mathbb{R}^8$, denoted E_8. This lattice belongs to the family of laminated lattices Λ_i, and is therefore sometimes denoted Λ_8. These laminated lattices form a series which starts with the triangular lattice in $2d$ (the densest lattice in $2d$). Λ_3 is obtained as a particular sequence of Λ_2 lattices packed in a third dimension, which gives the face centered cubic lattice, one of the two densest lattices in $3d$. Appropriately packing Λ_3 lattices along a fourth dimension leads to Λ_4, whose first shell is precisely the $\{3, 4, 3\}$ polytope we used above. Upon iteration, this construction eventually leads to the $\Lambda_8 = E_8$ lattice suitable for the two-qubit case. We shall focus here on the set of 240 sites belonging to the E_8 first shell that forms the Gosset polytope and, as for the one-qubit case, enumerate the physical states they represent.

3.2.1. Discrete Hopf fibration for the Gosset polytope on S^7

The 240 vertices of the Gosset polytope belong to the sphere S^7. These 240 vertices may be separated into ten equivalent subsets, each belonging to non-intersecting S^3 spheres. This is nothing but a discrete version of the S^7 Hopf fibration, with fibers S^3 and base $S^{4(13,16,18,19)}$.

It is simpler to use here quaternionic coordinates instead of complex or real ones. The above set T_1, scaled such that the corresponding points belong to a sphere S^3 of radius $1/\sqrt{2}$ now reads:

$$T_1 = \left\{ \pm\frac{1}{\sqrt{2}}, \pm\frac{\mathbf{i}}{\sqrt{2}}, \pm\frac{\mathbf{j}}{\sqrt{2}}, \pm\frac{\mathbf{k}}{\sqrt{2}}, \frac{1}{2\sqrt{2}}(\pm 1 \pm \mathbf{i} \pm \mathbf{j} \pm \mathbf{k}) \right\},$$

where $\mathbf{i}, \mathbf{j}$ and $\mathbf{k}$ are the standard unit quaternions. The set T_2 stays on a unit sphere and reads:

$$T_2 = \left\{ \frac{1}{\sqrt{2}}(\pm 1 \pm \mathbf{i}), \frac{1}{\sqrt{2}}(\pm 1 \pm \mathbf{j}), \frac{1}{\sqrt{2}}(\pm 1 \pm \mathbf{k}), \frac{1}{\sqrt{2}}(\pm \mathbf{i} \pm \mathbf{j}), \frac{1}{\sqrt{2}}(\pm \mathbf{i} \pm \mathbf{k}), \right.$$
$$\left. \frac{1}{\sqrt{2}}(\pm \mathbf{j} \pm \mathbf{k}) \right\}.$$

The 240 vertices of the Gosset polytope belong to the ten sets:

$$\begin{aligned} S_1 &= (T_2, 0), \quad S_2 = (0, T_2), \quad S_3 = (T_1, T_1), \quad S_4 = (T_1, -T_1), \\ S_5 &= (T_1, \mathbf{i}T_1), \quad S_6 = (T_1, -\mathbf{i}T_1), \quad S_7 = (T_1, \mathbf{j}T_1), \\ S_8 &= (T_1, -\mathbf{j}T_1), \quad S_9 = (T_1, \mathbf{k}T_1), \quad S_{10} = (T_1, -\mathbf{k}T_1). \end{aligned}$$

Each of the 10 sets gives a copy of a $\{3, 4, 3\}$ polytope on a fiber S^3. The points can be Hopf-mapped, as described elsewhere[13], onto the base space S^4. The location of the mapped point is intimately related to the entanglement of the corresponding two-qubit state. Indeed, the Hopf map is simply described as a first map which sends the pair (q_1, q_2) onto the quaternion $Q = \overline{q_1 q_2^{-1}}$ (which is sent to infinity if $q_2 = 0$), followed by an inverse stereographic map which sends Q to S^4. A main result is that the Hopf map is sensitive to entanglement: for separable states, Q is simply a complex number, not a generic quaternion; conversely, for maximally entangled states (MES), the purely complex part of Q vanishes. This translates onto the base S^4 in the following way. Embed S^4 into R^5, with coordinates $\{x_l, l = 0, \cdots, 4\}$; then separable states are such that $x_3 = x_4 = 0$, and the S^2 sphere spanned by $\{x_0, x_1, x_2\}$ form the standard Bloch sphere of the first qubit. Maximally entangled states map onto the unit circle in the

plane (x_3, x_4). Note that a well-known entanglement measure, the concurrence[20], is simply given by the radius in the plane (x_3, x_4): $c = \sqrt{x_3^2 + x_4^2}$, an expression which will be used later.

In the present case, it is then easy to verify that the sets S_1–S_6 correspond to separable states, while sets S_7–S_{10} correspond to maximally entangled states. The correspondence between vertices and states is made by transforming back the quaternion pairs into complex quadruplets whose terms are $(t_{00}, t_{01}, t_{10}, t_{11})$. More precisely, the (q_1, q_2) pair reads $(t_{00} + t_{01}\mathbf{j},\ t_{10} + t_{11}\mathbf{j})$. Note that the quaternion unit $\mathbf{j}$ acts on the right of the complex numbers, while it acts on the left in the definition of $S_{7,8}$. Since quaternion multiplication is non-commutative, this distinction is important in going back and forth between the lattice points and the states.

3.2.2. The separable states

Consider the set S_1, corresponding to the 24 states such that $t_{10} = t_{11} = 0$, and which reads

$$|0\rangle_1 \otimes |\Phi_l, \omega\rangle_2, \quad \omega = 0, \pi/2, \pi, 3\pi/2, \quad \text{and } l = 1, \ldots, 6.$$

As a whole, the six sets $S_1, \ldots, S_6$ encompass $6 \times 24 = 144$ vertices, forming altogether 36 physical states, with four values of the global phase for each qubit state. Note that the precise value of the phases are important here in order that our discretization procedure uniformly cover the full Hilbert space. Using the above defined eigenstates of the one-qubit Pauli matrices, these states read:

$\|\pm x\rangle \otimes \|\pm x\rangle\, e^{i(\pi/4 + m\pi/2)}$	$\|\pm x\rangle \otimes \|\pm y\rangle\, e^{i(\pi/4 + m\pi/2)}$	$\|\pm x\rangle \otimes \|\pm z\rangle\, e^{im\pi/2}$
$\|\pm y\rangle \otimes \|\pm x\rangle\, e^{i(\pi/4 + m\pi/2)}$	$\|\pm y\rangle \otimes \|\pm y\rangle\, e^{i(\pi/4 + m\pi/2)}$	$\|\pm y\rangle \otimes \|\pm z\rangle\, e^{im\pi/2}$
$\|\pm z\rangle \otimes \|\pm x\rangle\, e^{im\pi/2}$	$\|\pm z\rangle \otimes \|\pm y\rangle\, e^{im\pi/2}$	$\|\pm z\rangle \otimes \|\pm z\rangle\, e^{i(\pi/4 + m\pi/2)}$

where $m = 0, 1, 2, 3$ triggers the global phase. Each of the nine entries stands for the four possible sign combinations, leading to the announced 36 physical states. A simple view of these separable states consists in relating them to the "product" of two octahedra, each one belonging to the Bloch sphere of the individual qubits.

3.2.3. The maximally entangled states

The remaining four sets (altogether $4 \times 24 = 96$ sites) lead to a slightly more subtle structure. We find a total of 24 different physical MES, with four phase-distinct two-qubit states for each. But in the present case, the phase-distinct states actually belong to two different sets, either (S_7, S_8) or (S_9, S_{10}).

As an example, we consider the set S_7 and enumerate the states corresponding to, say, the quaternion pair $(1/\sqrt{2}, (1/\sqrt{2})\mathbf{j}) \in T_1$, which translates into the complex quadruplet $(1/\sqrt{2}, 0, 0, 1/\sqrt{2})$ and therefore to the MES:

$$|MES_1, 0\rangle = \frac{1}{\sqrt{2}}(|00\rangle + |11\rangle) = \frac{1}{\sqrt{2}}(|+z, +z\rangle + |-z, -z\rangle)\,.$$

The shortened notation $|+z, +z\rangle$ stands for $|+z\rangle_1 \otimes |+z\rangle_2$. There is only one other element in S_7, the pair $(-(1/\sqrt{2}), -(1/\sqrt{2})\mathbf{j})$, corresponding to $|MES_1, \pi\rangle = e^{i\pi}\,|MES_1, 0\rangle$. The other two elements belong to the set S_8 and read $(\mathbf{i}/\sqrt{2}, \mathbf{k}/\sqrt{2})$ and $(-(\mathbf{i}/\sqrt{2}), -(\mathbf{k}/\sqrt{2}))$, associated respectively to the states $|MES_1, \pi/2\rangle$ and $|MES_1, -\pi/2\rangle$. Before giving the full list of states, it is interesting to focus on the next three states in S_7, generated by $\mathbf{i}$, $\mathbf{j}$ and $\mathbf{k}$. One gets, respectively,

$$\begin{aligned}
|MES_2, 0\rangle &= \frac{\mathbf{i}}{\sqrt{2}}(|00\rangle - |11\rangle) = \frac{\mathbf{i}}{\sqrt{2}}(|+z, +z\rangle - |-z, -z\rangle)\,,\\
|MES_3, 0\rangle &= \frac{1}{\sqrt{2}}(|01\rangle + |10\rangle) = \frac{1}{\sqrt{2}}(|+z, -z\rangle + |-z, z\rangle)\,,\\
|MES_4, 0\rangle &= \frac{\mathbf{i}}{\sqrt{2}}(|01\rangle - |10\rangle) = \frac{\mathbf{i}}{\sqrt{2}}(|+z, -z\rangle - |-z, z\rangle)\,.
\end{aligned}$$

The set $\{|MES_1, 0\rangle\,, |MES_2, 0\rangle\,, |MES_3, 0\rangle\,, |MES_4, 0\rangle\}$ forms the entangled "magic" basis described elsewhere[21][22]. Each physical state $|MES_l\rangle$ corresponds to the four two-qubit states $|MES_l, \omega\rangle$, with $\omega = 0, \pi$ for states in S_7 and $\omega = \pi/2, -\pi/2$ for states in S_8. As a whole, the 48 vertices of the sets S_7 and S_8 provide 12 physical MES, each one representing a set of four phase-related states. They are listed below, in the $\omega = 0$ case, and with $\epsilon = e^{i\pi/4}$:

$$|MES_5,0\rangle = \frac{\epsilon}{2}(|00\rangle+|01\rangle)-\frac{\overline{\epsilon}}{2}(|10\rangle-|01\rangle)=\frac{\epsilon}{\sqrt{2}}(|+z,+x\rangle+\mathbf{i}\,|-z,-x\rangle),$$

$$|MES_6,0\rangle = \frac{\epsilon}{2}(|00\rangle-|10\rangle)+\frac{\overline{\epsilon}}{2}(|01\rangle+|11\rangle)=\frac{\epsilon}{\sqrt{2}}(|z,-y\rangle-|-z,y\rangle),$$

$$|MES_7,0\rangle = \frac{\overline{\epsilon}}{2}(|00\rangle-|10\rangle)+\frac{\epsilon}{2}(|01\rangle+|11\rangle)=\frac{\overline{\epsilon}}{\sqrt{2}}(|+z,+y\rangle-|-z,-y\rangle),$$

$$|MES_8,0\rangle = \frac{\overline{\epsilon}}{2}(|00\rangle+|01\rangle)-\frac{\epsilon}{2}(|10\rangle-|11\rangle)=\frac{\overline{\epsilon}}{\sqrt{2}}(|+z,+x\rangle-\mathbf{i}\,|-z,-x\rangle),$$

$$|MES_9,0\rangle = \frac{\epsilon}{2}(|00\rangle-|01\rangle)+\frac{\overline{\epsilon}}{2}(|10\rangle+|11\rangle)=\frac{\epsilon}{\sqrt{2}}(|+z,-x\rangle-\mathbf{i}\,|-z,x\rangle),$$

$$|MES_{10},0\rangle = \frac{\epsilon}{2}(|00\rangle+|10\rangle)-\frac{\overline{\epsilon}}{2}(|01\rangle-|11\rangle)=\frac{\epsilon}{\sqrt{2}}(|+z,+y\rangle+|-z,-y\rangle),$$

$$|MES_{11},0\rangle = \frac{\overline{\epsilon}}{2}(|00\rangle+|10\rangle)-\frac{\epsilon}{2}(|01\rangle-|11\rangle)=\frac{\overline{\epsilon}}{\sqrt{2}}(|+z,-y\rangle+|-z,y\rangle),$$

$$|MES_{12},0\rangle = \frac{\overline{\epsilon}}{2}(|00\rangle-|01\rangle)+\frac{\epsilon}{2}(|10\rangle+|11\rangle)=\frac{\overline{\epsilon}}{\sqrt{2}}(|+z,-x\rangle+\mathbf{i}\,|-z,x\rangle).$$

The latter 12 physical states may be read off from the two sets S_9 and S_{10}:

$$|MES_{13},0\rangle = \frac{1}{\sqrt{2}}|00\rangle+\frac{\mathbf{i}}{\sqrt{2}}|11\rangle=\frac{1}{\sqrt{2}}(|+z,+z\rangle+\mathbf{i}\,|-z,-z\rangle),$$

$$|MES_{14},0\rangle = \frac{\mathbf{i}}{\sqrt{2}}|00\rangle+\frac{1}{\sqrt{2}}|11\rangle=\frac{1}{\sqrt{2}}(\mathbf{i}\,|+z,+z\rangle+|-z,-z\rangle),$$

$$|MES_{15},0\rangle = \frac{1}{\sqrt{2}}|01\rangle-\frac{\mathbf{i}}{\sqrt{2}}|10\rangle=\frac{1}{\sqrt{2}}(|+z,-z\rangle-\mathbf{i}\,|-z,+z\rangle),$$

$$|MES_{16},0\rangle = \frac{\mathbf{i}}{\sqrt{2}}|01\rangle-\frac{1}{\sqrt{2}}|10\rangle=\frac{1}{\sqrt{2}}(\mathbf{i}\,|+z,-z\rangle-|-z,+z\rangle),$$

$$|MES_{17},0\rangle = \frac{\epsilon}{2}(|00\rangle+|01\rangle)-\frac{\mathbf{i}\overline{\epsilon}}{2}(|10\rangle-|11\rangle)=\frac{\epsilon}{\sqrt{2}}(|+z,+x\rangle-|-z,-x\rangle),$$

$$|MES_{18},0\rangle = \frac{\epsilon}{2}(|00\rangle-\mathbf{i}\,|10\rangle)+\frac{\overline{\epsilon}}{2}(|01\rangle+\mathbf{i}\,|11\rangle)=\frac{\epsilon}{\sqrt{2}}(|+z,-y\rangle-\mathbf{i}\,|-z,+y\rangle),$$

$$|MES_{19},0\rangle = \frac{\overline{\epsilon}}{2}(|00\rangle-\mathbf{i}\,|10\rangle)+\frac{\epsilon}{2}(|01\rangle+\mathbf{i}\,|11\rangle)=\frac{\overline{\epsilon}}{\sqrt{2}}(|+z,+y\rangle-\mathbf{i}\,|-z,-y\rangle),$$

$$|MES_{20},0\rangle = \frac{\overline{\epsilon}}{2}(|00\rangle+|01\rangle)-\frac{\mathbf{i}\epsilon}{2}(|10\rangle-|11\rangle)=\frac{\overline{\epsilon}}{\sqrt{2}}(|+z,+x\rangle+|-z,-x\rangle),$$

$$|MES_{21},0\rangle = \frac{\epsilon}{2}(|00\rangle-|01\rangle)+\frac{\mathbf{i}\overline{\epsilon}}{2}(|10\rangle+|11\rangle)=\frac{\epsilon}{\sqrt{2}}(|+z,-x\rangle+|-z,x\rangle),$$

$$|MES_{22},0\rangle = \frac{\epsilon}{2}(|00\rangle+\mathbf{i}\,|10\rangle)-\frac{\overline{\epsilon}}{2}(|01\rangle-\mathbf{i}\,|11\rangle)=\frac{\epsilon}{\sqrt{2}}(|+z,+y\rangle+\mathbf{i}\,|-z,-y\rangle),$$

$$|MES_{23}, 0\rangle = \frac{\overline{\epsilon}}{2}(|00\rangle + \mathbf{i}\,|10\rangle) - \frac{\epsilon}{2}(|01\rangle - \mathbf{i}\,|11\rangle) = \frac{\overline{\epsilon}}{\sqrt{2}}(|+z, -y\rangle + \mathbf{i}\,|-z, y\rangle),$$

$$|MES_{24}, 0\rangle = \frac{\overline{\epsilon}}{2}(|00\rangle - |01\rangle) + \frac{\mathbf{i}\epsilon}{2}(|10\rangle + |11\rangle) = \frac{\overline{\epsilon}}{\sqrt{2}}(|+z, -x\rangle - |-z, x\rangle).$$

Succinctly, the 96 two-qubit entangled states can be written:

$$|MES_l, \omega\rangle = e^{i\omega}\,|MES_l, 0\rangle, \quad \text{with } \omega = 0, \pi/2, \pi, 3\pi/2 \text{ and } l = 1, \ldots, 24.$$

Modding out the global phase, we can write the 24 physical states in the form:

$\frac{1}{\sqrt{2}}\left(\|+z, +z\rangle + e^{i\theta}\,\|-z, -z\rangle\right)$	$\frac{1}{\sqrt{2}}\left(\|+z, -z\rangle + e^{i\theta}\,\|-z, z\rangle\right)$
$\frac{1}{\sqrt{2}}\left(\|+z, +x\rangle + e^{i\theta}\,\|-z, -x\rangle\right)$	$\frac{1}{\sqrt{2}}\left(\|+z, -x\rangle + e^{i\theta}\,\|-z, +x\rangle\right)$
$\frac{1}{\sqrt{2}}\left(\|+z, +y\rangle + e^{i\theta}\,\|-z, -y\rangle\right)$	$\frac{1}{\sqrt{2}}\left(\|+z, -y\rangle + e^{i\theta}\,\|-z, +y\rangle\right)$

with $\theta = 0, \pi/2, \pi, 3\pi/2$.

Note that these 24 entangled states, together with the above 36 separable states, are in one-to-one correspondence, up to a global phase, with the 60 discrete states on $\mathfrak{H}_2$ presented in Section 2.

3.3. Comments

3.3.1. Finer discretizations of H_2: higher E_8 shells

Thus far, this alternate technique has provided compelling confirmation of the results from Section 2. However, the present purely geometric approach does not describe the discrete set's transformation group. This point could be in principle addressed, albeit in a much less transparent way than in the first part of this paper, by using the E_8 lattice point group (which has a high order) and finding the subgroup of rotations which survive the Hopf map. But this lattice approach does have the benefit of allowing discrete sets with a finer minimum distance (i.e., $0 < d_{jk} < \pi/2$) to be explored in a straightforward manner: while the first shell of E_8 provides the discrete set with a minimum distance of $\pi/2$, a finer discretization might be achieved by considering the higher order shells in E_8. This construction would provide a uniform set of two-qubit states, some of which would have intermediate entanglement. A note of caution is in order here, since we are only interested in describing normalized quantum states. Lattice points which are aligned, as viewed from the origin, contribute to the same two-qubit state. One should therefore only focus on the "visible points," which form the lattice's Möbius transform[23].

We do not give here a detailed description of these finer discretizations of H_2. However, we note that the number M_J of sites on the Jth shell around an E_8 vertex is simply given by(?)

$$M_J = 240 \sum_{d|J} d^3,$$

where d denotes integers which divide J. The table below displays these numbers for the first four shells. Again, the physical states are obtained from these two-qubit states by modding out a global phase.

J	1	2	3	4
M	240	2160	6720	17520

The shell by shell analysis, and its relation to the Hopf map, was done elsewhere[16,18]. It allows us to get points on the second shell corresponding to states having concurrence $0, 1/2, 1/\sqrt{2}, 1$. The third shell contributes states of concurrence 0, 1/3, 2/3, $\sqrt{5}/3$, $\sqrt{8}/3$ and 1.

3.3.2. Discrete one-qubit mixed states

A second advantage of our lattice approach over the pseudostabilizer approach is that it allows a discussion of discrete sets of *mixed* states. It is well known that the full set of one-qubit mixed states can be obtained by tracing out one qubit of generic two-qubit pure states. Mixed states are represented by points inside the so-called "Bloch ball," bounded by the pure-state Bloch sphere. In the context of generalizing the Bloch sphere for two-qubit pure states using the S^7 Hopf fibration[13], it was shown that the Bloch ball corresponds precisely to the restriction to the triplet (x_0, x_1, x_2) on the base space S^4. This describes mixed states obtained upon tracing out the second qubit. With this in mind, we are tempted to propose, in parallel to the two-qubit pure state discretization, an E_8-related discretization of the Bloch ball.

From the E_8 first shell, one gets the six permutations $(\pm 1, 0, 0)$, corresponding to pure states on the Bloch sphere (the traced separable two-qubit states) forming an octahedron. But one also gets the point $(0, 0, 0)$, the Bloch ball center, corresponding to traced maximally entangled states. Then, from the E_8 second shell, we find in addition the eight permutations $(\pm\frac{1}{2}, \pm\frac{1}{2}, \pm\frac{1}{2})$—a cube of radius $\sqrt{3}/2$—and the twelve permutations $(\pm\frac{1}{2}, \pm\frac{1}{2}, 0)$—a cuboctahedron of radius $1/\sqrt{2}$. The Bloch ball can be further discretized by using traced states originating from higher E_8 shells.

3.3.3. Conclusion to Section 3

We have presented a second technique for producing a uniform discrete set of states from the continuous Hilbert space, again focusing on the one- and two-qubit cases. The pseudostabilizer and dense lattice strategies were done independently, and their agreement provides a compelling confirmation of our results, while also calling for a better understanding of their possible deeper relationship. While the dense lattice strategy is less easily focused on the transformation groups leaving the discrete sets invariant, it does have the advantage of allowing a discussion of discrete sets with a smaller minimum distance between states, and also of discrete sets of mixed states. Looking ahead, a discretization of higher-dimensional Hilbert spaces may be achieved in the dense lattice approach by using high-dimensional lattices in 2^N dimensions[24]. Though it does not describe the entanglement properties as nicely as in the two-qubit case, the S^{15} Hopf map, corresponding to the three-qubit case, has been found to be entanglement -sensitive[25,26]. This case should be related to the dense lattice Λ_{16} in $\mathbb{R}^{16}$, and is presently under study. It is interesting to note that the number of lattice sites closest to the origin—the lattice "kissing number"—for this case is 4320, which is precisely four times the expected number of vertices on the uniform Hilbertian polytope $\mathfrak{H}_3$. We are therefore likely to face a similar situation as in the one- and two-qubit cases, where there were four phase-related qubit states associated with each physical state. However, the four-to-one relation between the Λ_{16} first shell sites and the vertices of $\mathfrak{H}_3$ remains to be checked. Generalization to more than three qubits cannot use the Hopf fibrations, limited to S^{15}. A particularly interesting family to be checked further is the one described long ago by John Leech[27], which coincides with those studied here for $N = 1, 2$ and 3, and whose kissing number is, for any N, precisely four times that given in the first part of this paper for the number of states in the generic Hilbertian polytopes. As for the three-qubit case, this precise four-to-one relation remains to be checked.

4. ACKNOWLEDGMENTS

M. D. and C. R. are indebted to Ike Chuang for his enthusiastic teaching of quantum information theory and to Daniel Gottesman for communicating and explaining his results. In addition, R. M. would like to thank Perola Milman and Karol Zyczkowski for interesting discussions and comments on the two-qubit Hilbert space geometry, and Philippe Biane who, while reading the first version of this manuscript, drew his atten-

tion to John Leech's 1964 paper. Daniel Esteve and Denis Vion are also gratefully acknowledged by all of us for helpful interactions. Finally, John Preskill's web-accessible notes and exercises on quantum information have been very useful. This work has been supported by the ARO/ARDA grant DAAD190210044.

REFERENCES

1. P. W. Shor, in Proceedings, of the 35th *Annual Symposium on Foundations of Computer Science* (IEEE Press, Los Alamitos, CA, 1994).
2. D. Gottesman, *Phys. Rev. A* **54**, 1862 (1996).
3. A. M. Steane, *Phys. Rev. Lett.* **77**, 793 (1996).
4. P. Shor, *Phys. Rev. A* **52**, 2493 (1995).
5. M. A. Nielsen and I. L. Chuang, *Quantum Computation and Quantum Information* (Cambridge University Press, Cambridge, 2000), Chap. 10.
6. H. K. Cummins, G. Llewellyn, and J. A. Jones, *Phys. Rev. A* **67**, 042308 (2003), and references therein.
7. Vandersypen *et al., Nature* **414**, 883 (2001).
8. A. C. Dohert *et al., Phys. Rev. A* **62**, 012105 (2000).
9. C. Ahn, A. C. Doherty, and A. J. Landahl, *Phys. Rev. A* **65**, 042301 (2002).
10. D. Gottesman, personal communication.
11. D. Gottesman, arXiv e-print quant-ph/9807006.
12. D. Gottesman, *Stabilizer Codes and Quantum Error Correction.* Ph.D. thesis, California Institute of Technology, Pasadena, CA (1997). arXiv e-print quant-ph/9705052.
13. R. Mosseri and R. Dandoloff, *J. Phys. A: Math. Gen.* **34**, 10243–10252 (2001).
14. M. Kus and K. Zyczkowski, *Phys. Rev. A* **63**, 032307 (2001).
15. H. Urbanke, *Am. J. Phys.* **59**, 53 (1991).
16. J. F. Sadoc and R. Mosseri, *Geometric Frustration* (Cambridge University Press, Cambridge, 1999).
17. H. S. M. Coxeter, *Regular Polytopes* (Dover, New York, 1973).
18. J. F. Sadoc and R. Mosseri, *J. Phys. A: Math. Gen.* **26**, 1789–189 (1993).
19. N. S. Manton, *Common Math. Phys.* **113**, 341–351 (1987).
20. W. K. Wootters, *Phys. Rev. Lett.* **80**, 2245 (1998).
21. C. H. Bennett, D. P. DiVincenzo, J. Smolin, and W. K. Wootters, *Phys. Rev. A* **54**, 3824 (1996).
22. S. Hill. and W. K. Wootters, *Phys. Rev. Lett.* **78**, 5022 (1997).
23. R. Mosseri, *J. Phys. A: Math. Gen.* **25**, L25–L29 (1992).
24. V. Elser and N. J. A. Sloane, *J. Phys. A: Math. Gen.* **20**, 6161–6168 (1987).
25. R. Mosseri, quant-ph/0310053.
26. B. A. Bernevig and H. D. Chen, *J. Phys. A: Math. Gen.* **36**, 8325 (2003).
27. J. Leech, *Can. J. Math.* **16**, 657–682 (1964).